

Identification of denatured and normal biological tissues based on compressed sensing and refined composite multi-scale fuzzy entropy during high intensity focused ultrasound treatment

Shang-Qu Yan(颜上取), Han Zhang(张含), Bei Liu(刘备), Hao Tang(汤昊), and Sheng-You Qian(钱盛友)

Citation: Chin. Phys. B, 2021, 30 (**2**): 028704. DOI: 10.1088/1674-1056/abcfa7
Journal homepage: http://cpb.iphy.ac.cn; http://iopscience.iop.org/cpb

What follows is a list of articles you may be interested in

Super-resolution filtered ghost imaging with compressed sensing

Shao-Ying Meng(孟少英), Wei-Wei Shi(史伟伟), Jie Ji(季杰), Jun-Jie Tao(陶俊杰), Qian Fu(付强), Xi-Hao Chen(陈希浩), and Ling-An Wu(吴令安)

Chin. Phys. B, 2020, 29 (**12**): 128704. DOI: 10.1088/1674-1056/abc15f

Novel Fourier-based iterative reconstruction for sparse fan projection using alternating direction total variation minimization

Zhao Jin(金朝), Han-Ming Zhang(张瀚铭), Bin Yan(闫镔), Lei Li(李磊), Lin-Yuan Wang(王林元), Ai-Long Cai(蔡爱龙)

Chin. Phys. B, 2016, 25 (**3**): 038701. DOI: 10.1088/1674-1056/25/3/038701

Applicability of initial optimal maternal and fetal electrocardiogram combination vectors to subsequent recordings

Yan Hua-Wen, Huang Xiao-Lin, Zhao Ying, Si Jun-Feng, Liu Tie-Bing, Liu Hong-Xing

Chin. Phys. B, 2014, 23 (**11**): 118702. DOI: 10.1088/1674-1056/23/11/118702

Cardiac electrical activity imaging of patients with CRBBB or CLBBB in magnetocardiography

Zhu Jun-Jie, Jiang Shi-Qin, Wang Wei-Yuan, Zhao Chen, Wu Yan-Hua, Luo Ming, Quan Wei-Wei

Chin. Phys. B, 2014, 23 (**4**): 048702. DOI: 10.1088/1674-1056/23/4/048702

Magnetic nanoparticle-based cancer nanodiagnostics

Muhammad Zubair Yousaf, Yu Jing, Hou Yang-Long, Gao Song

Chin. Phys. B, 2013, 22 (**5**): 058702. DOI: 10.1088/1674-1056/22/5/058702

Identification of denatured and normal biological tissues based on compressed sensing and refined composite multi-scale fuzzy entropy during high intensity focused ultrasound treatment*

Shang-Qu Yan(颜上取)[1], Han Zhang(张含)[1], Bei Liu(刘备)[2], Hao Tang(汤昊)[1], and Sheng-You Qian(钱盛友)[1,†]

[1] School of Physics and Electronics, Hunan Normal University, Changsha 410081, China
[2] College of Mathematics and Physics, Hunan University of Arts and Science, Changde 415000, China

(Received 16 September 2020; revised manuscript received 26 October 2020; accepted manuscript online 2 December 2020)

In high intensity focused ultrasound (HIFU) treatment, it is crucial to accurately identify denatured and normal biological tissues. In this paper, a novel method based on compressed sensing (CS) and refined composite multi-scale fuzzy entropy (RCMFE) is proposed. First, CS is used to denoise the HIFU echo signals. Then the multi-scale fuzzy entropy (MFE) and RCMFE of the denoised HIFU echo signals are calculated. This study analyzed 90 cases of HIFU echo signals, including 45 cases in normal status and 45 cases in denatured status, and the results show that although both MFE and RCMFE can be used to identify denatured tissues, the intra-class distance of RCMFE on each scale factor is smaller than MFE, and the inter-class distance is larger than MFE. Compared with MFE, RCMFE can calculate the complexity of the signal more accurately and improve the stability, compactness, and separability. When RCMFE is selected as the characteristic parameter, the RCMFE difference between denatured and normal biological tissues is more evident than that of MFE, which helps doctors evaluate the treatment effect more accurately. When the scale factor is selected as 16, the best distinguishing effect can be obtained.

Keywords: compressed sensing, high intensity focused ultrasound (HIFU) echo signal, multi-scale fuzzy entropy, refined composite multi-scale fuzzy entropy

PACS: 87.85.−d, 05.45.−a **DOI:** 10.1088/1674-1056/abcfa7

1. Introduction

High intensity focused ultrasound (HIFU) therapy is a non-invasive tumor treatment technology in clinical medicine.[1,2] It focused the ultrasonic energy on the irradiation region, which leads to cancer cell death in the target region without damage to the surrounding normal cell.[3,4] Therefore, it is essential to monitor the effect of HIFU treatment to ensure the safety and efficiency of HIFU treatment. At present, computed tomography (CT), magnetic resonance imaging (MRI), ultrasound images, and ultrasound signals are usually used for HIFU treatment monitoring.[5–8] However, the CT is based on x-ray technology, and the ionizing radiation of x-ray is harmful to the human body. The MRI scan takes a long time and is sensitive to the patient's body movement, which is easy to produce artifacts. The ultrasound images are converted from the ultrasound signals, and part of the information will be lost during the conversion process, resulting in an inaccurate diagnosis.[9] The ultrasound signals have become the research hotspot field due to their good accuracy, real-time performance, low cost, and strong compatibility.[10] In this paper, the method proposed is directly based on HIFU echo signals and the nonlinear characteristics of HIFU echo signals.

During HIFU treatment, the HIFU echo signals are polluted by noise because of the experimental environment and operations, so the signals should be denoised before any other processing. In recent years, many researchers have conducted denoising studies on nonlinear time series. Inspired by Donoho,[11] Chen *et al.*,[12] and Ramdas *et al.*,[13] the denoising method of HIFU echo signals based on compressed sensing (CS) is proposed. CS can transform the signal from the time domain to the sparse domain and then reconstruct the signal, which can retain the useful information of the signal and remove the noise.[14,15]

The HIFU echo signal is nonlinear. When biological tissues are denatured, some characteristics of the HIFU echo signal change. Biological tissues exhibit different nonlinear characteristics due to denaturation. In order to extract the nonlinear characteristics of biological tissues, the researchers initially analyzed the sample entropy (SE) but encountered difficulty, because SE involved any two coarse-grained time series whose similar distance exceeds a fixed value for calculation, which may easily lead to instability of SE.[16] Other researchers proposed approximate entropy (AE) for analysis. However, when the data length of the signal is short, AE is lower than the expected value, and the correlation is poor.[17,18] In order to solve these shortcomings, fuzzy entropy (FE) is proposed. FE introduces an exponential function to determine the similarity be-

*Project supported by the National Natural Science Foundation of China (Grant Nos. 11774088 and 11474090).
†Corresponding author. E-mail: shyqian@hunnu.edu.cn
© 2021 Chinese Physical Society and IOP Publishing Ltd

tween two arbitrary time series. However, FE still reflects the complexity and irregularity of the signal on a single scale, and it is difficult to reflect all the characteristics of the signal.[19,20] So a method called multi-scale fuzzy entropy (MFE) is proposed to solve this problem.[21–23] At the same time, with the scale factor increases, the length of the time series becomes shorter, resulting in a sudden change of MFE. In order to alleviate this drawback, inspired by Fadlallah *et al.*,[24] Wu *et al.*,[25,26] and Zheng *et al.*,[27] a new nonlinear analysis algorithm, called refined composite multi-scale fuzzy entropy (RCMFE), is proposed. RCMFE averages MFE to reduce the entropy fluctuation and the generation of uncertain entropy, thereby improving the stability and reliability of MFE.

In this paper, it is proposed to use CS and RCMFE to identify denatured porcine tissues. Firstly, CS is used to denoise the HIFU echo signal. Then RCMFE is used to analyze the denoised HIFU echo signal to obtain the nonlinear difference between normal and denatured porcine tissues, to better monitor and evaluate HIFU treatment to ensure its safety and effectiveness, and in the clinical direction to provide certain help for the doctor.

2. Theory

2.1. Compressed sensing

In 2006, Donoho proposed the compressed sensing (CS) theory, which suggested that if the signal is sparse or nearly sparse, it can be reconstructed by sampling points much lower than the requirements of the Nyquist sampling theorem.[11] CS theory mainly includes the following three parts:

1) Sparse representation of signal: when a signal is not sparse in the time domain, the one-dimensional signal $X_{N\times 1}$ should be converted into a sparse domain Ψ, which is K-sparse in the sparse domain Ψ ($K \ll N$). The process is

$$f = \Psi X, \tag{1}$$

where f is the sparse representation of X in the sparse domain; Ψ is the sparse domain; X is the $N \times 1$ dimensional signal.

Discrete cosine transform (DCT) and fast Fourier transform (FFT) are commonly used to obtain the sparse expression of the original signal X in the sparse domain Ψ. In this paper, FFT is used to obtain the sparse expression f.

2) Compression observation of signal: an appropriate observation matrix Φ is selected for observation, and the observation value $y = \{y_1, y_2, \ldots, y_M\}$ is obtained. The process is

$$y = \Phi\Psi X = \Theta X, \tag{2}$$

where Φ is the $M \times N$ dimension observation matrix; M is the data length of the original signal after down-sampled; Θ is the perception matrix. Both the observation matrix Φ and the perception matrix Θ need to satisfy the restricted isometry property (RIP).[28]

Usually, the Gaussian random observation matrix can become the observation matrix Φ. However, in practical engineering applications, although the Gaussian random observation matrix has good uncorrelation, its unstructured nature causes problems that are difficult to implement and increase the computational complexity, which slows down the reconstruction process. Therefore, inspired by the structured principle, a sparse cyclic structured matrix with low complexity is constructed, which is easy to implement and has high uncorrelation.[29] The construction process is as follows:

Step 1. Firstly, a $1 \times N$ dimensional zero-row vector O is constructed, and then a diagonal matrix E of $N \times N$ dimensional only containing ± 1 is constructed, where N is the data length of the original signal.

Step 2. The K positions of the zero vector O are randomly selected, and 0 is changed to 1 ($K < N$) to obtain a 0–1 sparse vector A, and then the right cyclic displacement of A is M bits to obtain a sparse matrix A_1. Where each right cyclic displacement is saved as a row in A_1, and the final size of A_1 is $M \times N$. M is the data length of the original signal after the down-sampled.

Step 3. The sparse matrix A_1 is multiplied by the random diagonal matrix E to obtain the observation matrix Φ.

3) Reconstruction of signal: the observation value y and the reconstruction algorithm are used to obtain the reconstructed signal. In this paper, the reconstruction algorithm used regularized orthogonal matching pursuit (ROMP). Compared with orthogonal matching pursuit (OMP), the advantage of the ROMP algorithm is that K atoms can be selected in each iteration, and the atoms selected each time can be screened again through the regularization principle to remove atoms with lower energy and improve accuracy.[30,31]

2.2. Multi-scale fuzzy entropy

The concept of multi-scale is introduced based on fuzzy entropy, and it is used to describe the complexity of time series on different time scales. The calculation method is as follows:

1) The original time series $X = \{x_1, x_2, \ldots, x_b, \ldots, x_N\}$ is subject to coarse-grained conversion on the original time series to obtain a new sequence

$$x_a^{(\tau)} = \frac{1}{\tau} \sum_{b=(a-1)\tau+1}^{a\tau} x_b, \quad 1 \leqslant a \leqslant N/\tau, \tag{3}$$

where τ is the scale factor. When $\tau = 1$, $\{x_a^{(\tau)}\}$ is the original data $\{x_b\}$; when $\tau > 1$, the original data is divided into coarse-grained sequence $\{x_a^{(\tau)}\}$ whose length does not exceed N/τ.

2) The embedding dimension m is determined, and the sequence is spatially reconstructed

$$X_i^m = \{x(i), x(i+1), \ldots, x(i+m-1)\} - u_0(i), \quad (i = 1, \ldots, N/\tau - m + 1), \tag{4}$$

where u_0 is defined as the mean of m consecutive samples starting at the i-th point $u_0(i) = \frac{1}{m}\sum_{j=0}^{m-1} x(i+j)$, and $x(i+k)$ is the $(i+k)$ term of $\left\{x_a^{(\tau)}\right\}$. When m is 1, the length of the new sequence is the same as that of the coarse-grained sequence, and when m is 2, the length of the new sequence is $N/\tau - 1$, which leads to insufficient information of multi-scale entropy. However, when m is too large, the coupling between data will be reduced. Therefore, the embedded dimension m is usually taken as 3, 4, 5.

3) The distance d_{ij}^m between the vector X_i and the vector X_j is defined as the maximum difference between the corresponding elements of the two vectors

$$d_{ij}^m = \max |x(i+k) - x(j+k)|. \tag{5}$$

4) The similarity of two vectors D_{ij}^m is defined by the degree of fuzzy membership function $\mu = (x, r)$,

$$D_{ij}^m = \mu(d_{ij}^m, r) = \exp\left[-\frac{(d_{ij}^m)^2}{r}\right], \tag{6}$$

where $\mu = (x, r)$ is a fuzzy membership function in exponential form, r and 2 are the width and gradient of the boundary, respectively.

5) $A_m(r)$ is a sub-function of the fuzzy function, which is defined as

$$A_m(r) = \frac{1}{N-m}\sum_{i=1}^{N-m}\left|\frac{1}{N-m-1}\sum_{j=1,\, j\neq i}^{N-m} D_{ij}\right|. \tag{7}$$

6) Similarly, the embedding dimension of the model is determined to be $m+1$, and repeat the steps 1)–step 5) to get $A_{m+1}(r)$.

7) The multi-scale fuzzy entropy of the time series is defined as follows:

$$\mathrm{MFE}(m, \tau, r, N) = \mathrm{FuzzyEn}(m, r, x_a^{(\tau)}), \tag{8}$$

where $\mathrm{FuzzyEn}(m, r, N) = -\mathrm{In}\frac{A_{m+1}}{A_m}$.

2.3. Refined composite multi-scale fuzzy entropy

As the scale factor τ increased, the length of the sequence decreased, and multi-scale entropy calculation of the short sequence may cause sudden changes. Therefore, Wu *et al.* proposed a new method called RCMSE to improve the accuracy of MSE.[26] In this paper, we introduced the concept of refined composite into MFE, then CMFE and RCMFE are proposed. The CMFE value is calculated by

$$\begin{aligned}\mathrm{CMFE}(m, \tau, r, N) &= \frac{1}{\tau}\sum_{a=1}^{\tau}\mathrm{FuzzyEn}\left(m, r, x_a^{(\tau)}\right) \\ &= \frac{1}{\tau}\sum_{a=1}^{\tau}\left(-\mathrm{In}\frac{A_{m+1}}{A_m}\right).\end{aligned} \tag{9}$$

CMFE defines the average value of the logarithm in MFE. Compared with MFE, CMFE algorithm has higher estimation accuracy. However, in the process of CMFE calculation, the probability of generating uncertain entropy is relatively greater. Therefore, RCMFE is proposed to solve this problem. The algorithm is as follows:

$$\begin{aligned}\mathrm{RCMFE}(m, \tau, r, N) &= -\mathrm{In}\left(\frac{\overline{A_{m+1}}}{\overline{A_m}}\right) \\ &= -\mathrm{In}\left(\frac{\frac{1}{\tau}\sum_{a=1}^{\tau} A_{m+1}}{\frac{1}{\tau}\sum_{a=1}^{\tau} A_m}\right) = -\mathrm{In}\left(\frac{\sum_{a=1}^{\tau} A_{m+1}}{\sum_{a=1}^{\tau} A_m}\right).\end{aligned} \tag{10}$$

2.4. Intra-class distance and inter-class distance

Inspired by Kira and Rendell, we used intra-class distance and inter-class distance as evaluation indicators.[32] The intra-class distance and the inter-class distance are widely used as indicators for feature selection of image recognition, biological information recognition, and gear wear signal recognition.[33,34] The compactness and separability of tissues status are better when the intra-class distance is smaller, and the inter-class distance is larger.

The calculation formulas of the intra-class distance and the inter-class distance are as follows:[32]

$$D_{\mathrm{intra}} = \sqrt{1\Big/k\sum_{j=1}^{k}\left[\frac{1}{k-1}\sum_{\substack{i=1\\ i\neq j}}^{k}\sum_{k=1}^{n}(a_k^j - a_k^i)^2\right]}, \tag{11}$$

$$D_{\mathrm{inter}} = \sqrt{\sum_{k=1}^{n}(m_{1k} - m_{2k})^2}, \tag{12}$$

where $\{a(i)\ |i = 1, 2, \ldots k\}$ is the sample set for each mode in n-dimensional space, then m_{1k} and m_{2k} are the k-th components of two types of the sample sets.

3. Experimental methods and results

3.1. Experimental system

The HIFU experimental system is shown in Fig. 1. Before the experiment, the experiment environment and fresh porcine muscle tissues should be prepared. The 95% ethanol was mixed with povidone at a ratio of 4 : 1, then the mixture was poured into a water tank and mixed with water at a ratio of 1 : 20 to remove oxygen, and waited an hour before the experiment to stabilize the mixture. The fresh porcine muscle tissues

were fixed on an acoustic rubber plate and immersed in the mixture under the HIFU source (PRO2008, Shenzhen, China). The position change of the HIFU irradiation target region can be controlled by a 3D position system of the computer. At the top of the HIFU transducer, a channel allowed the passage of a hydrophone probe (FOPH2000, Leutenbach, DE). The temperature of porcine tissues was measured by the thermocouple (DT-3891G, Shenzhen, China) to estimate the degree of injury in the HIFU treatment target region. The HIFU echo signals were received by a hydrophone probe, and then they were amplified by a broadband signal amplifier and sent to a digital oscilloscope (MDO3032, Tektronix, USA) for observation and preservation. In this paper, the central frequency of the HIFU echo signal is 1.39 MHz, the second harmonic frequency is 2.78 MHz, and the number of data points is 10000. The 90 groups of HIFU echo signals are obtained from 10 groups of fresh porcine muscle tissues, and it consists of 45 normal status and 45 denatured status. The HIFU echo signals are polluted by noise due to the influence of measuring equipment and environmental factors, so these signals should be denoise first.

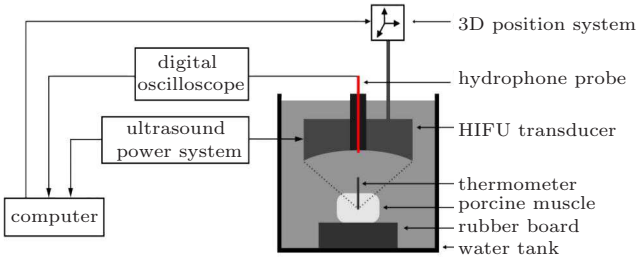


Fig. 1. Experimental system.

3.2. HIFU echo signal denoising based on compressed sensing

The sparsity of signal is one of the preconditions for using compressed sensing. However, the actual signal is not sparse in the time domain, so it is necessary to use Eq. (1) to convert the non-sparsity signal into the sparse signal. Figure 2(a) is the waveform and spectrum of HIFU echo signal in normal status. It can be seen that the signal waveform is not sparse and cannot be performed with compressed sensing. Therefore, FFT is used to transform the HIFU echo signal from the time domain to the spectrum. The central frequency and the second harmonic can be observed clearly from the spectrum. Although there are other noise frequencies, these amplitudes are small, and the condition of approximate sparsity can be met.

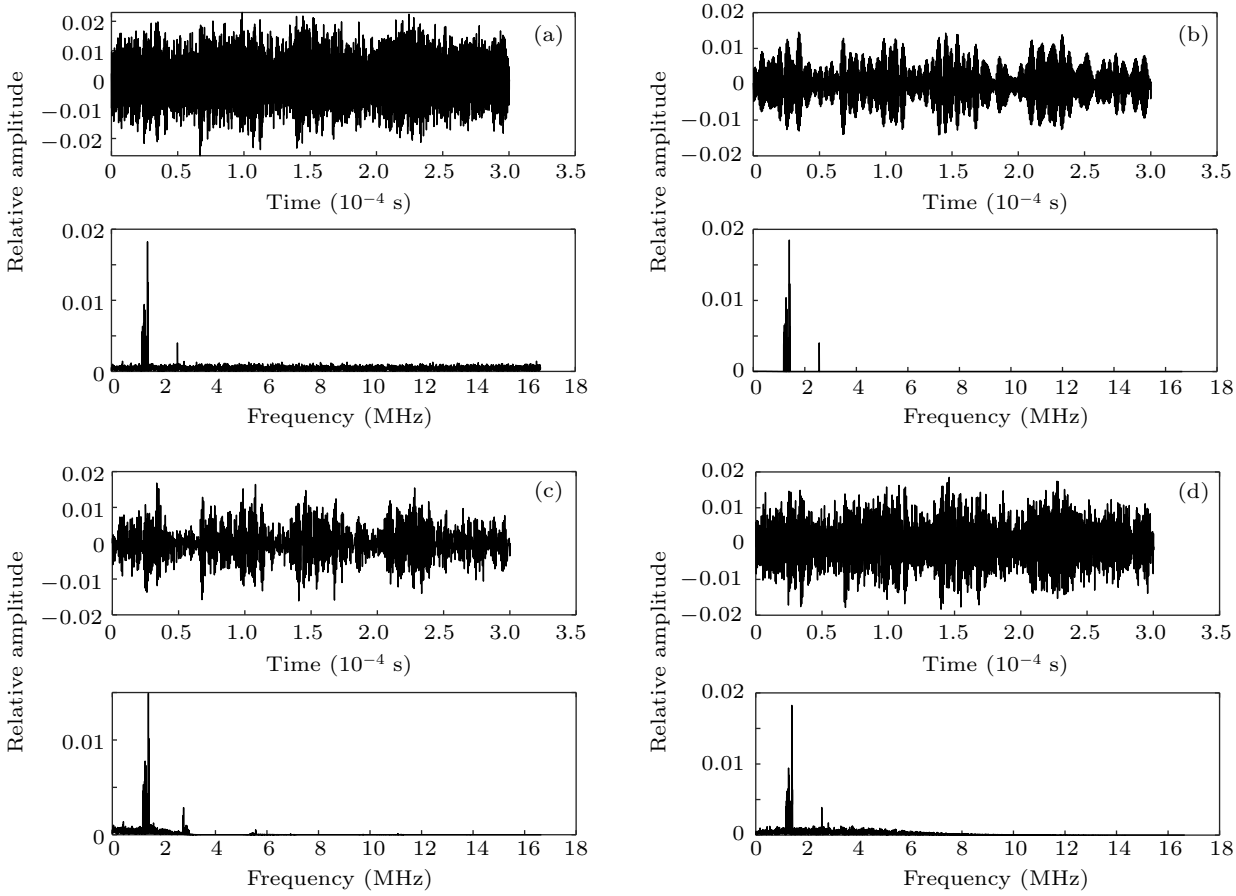


Fig. 2. The waveform and spectrum of HIFU echo signal and its denoising signal. (a) the HIFU echo signal; (b) the CS denoising; (c) the wavelet denoising; (d) the EMD denoising.

Therefore, the spectrum is used as the sparse domain Ψ for compressed sensing. We take 20% of the original signal data for reconstruction. In order to show the superiority of the CS method, the wavelet denoising method and empirical mode decomposition (EMD) denoising method are used for comparison. In the wavelet denoising method, the 'sym6' is selected as the wavelet basis for five-layer decomposition, and 'rigorous SURE' is selected for threshold estimation.

Figures 2(c) and 2(d) show the waveform and spectrum after wavelet denoising and EMD denoising, respectively, and it can be seen that noises still exist in the low-frequency part of these spectrums. Because of these low-frequency noises, their waveforms are different from Fig. 2(b). The wavelet denoising effect is depended on the wavelet basis and decomposition layer number. There is an end-point effect in the EMD denoising method, which leads to a poor denoising effect near the center frequency and the second harmonic.

As shown in Fig. 2(b), the spectrum after CS denoising only keeps the main characteristic. Therefore, MFE and RCMFE of the HIFU echo signals after CS denoising are extracted for further research.

3.3. Simulation analysis of MFE and RCMFE

This section compares MFE with RCMFE for the white Gaussian noise of the 10000-point data. We selected the embedding dimension $m = 3, 4, 5$, similar tolerance $r = 0.1\times$ standard deviation of the time series, and delay time as 1. Figure 3 shows the difference between MFE and RCMFE of the simulated signals under various scale factors.

Figures 3(a)–3(c) are the entropy values of the simulated signals with embedding dimension $m = 3,4,5$.

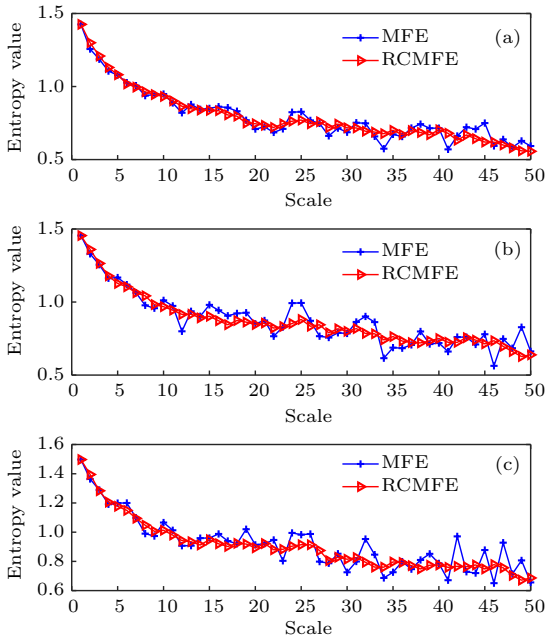


Fig. 3. MFE and RCMFE of white Gaussian noise under various scale factors. (a) $m = 3$; (b) $m = 4$; (c) $m = 5$.

When the scale factor increases, the entropy fluctuation range increases, and RCMFE reduces the entropy fluctuation relative to MFE, which makes it decline steadily and improves the stability and reliability. Table 1 shows the standard deviation of the three embedding dimensions, and it can be seen from the table that RCMFE has a smaller standard deviation than MFE.

Table 1. Results of the standard deviation.

Entropy categories	Embedding dimension		
	$m = 3$	$m = 4$	$m = 5$
MFE	0.1805	0.1818	0.1832
RCMFE	0.1760	0.1798	0.1809

3.4. Selection of appropriate embedding dimension

To analyze the most appropriate embedding dimension m in the denoised HIFU echo signals, we used 18 groups of denoised HIFU signals (9 groups of denatured status and 9 groups of normal status) to compare the entropy with three embedding dimensions. Figure 4 compares MFE and RCMFE with three embedded dimensions under scale factor 1–20, and the embedded dimensions of each row are the same. As shown in Fig. 4, when the embedded dimension m increases, the entropy fluctuation of MFE and RCMFE increases, but RCMFE reduces the fluctuation of entropy, which means that the improvement is effective. When the embedded dimension is 3, the entropy difference between denatured and normal tissues is greater than that of the other two embedding dimensions, and the variance is also smaller than the other two embedding dimensions. Therefore, in the follow-up study, the embedding dimension m takes 3 as the most appropriate embedding dimension.

3.5. MFE and RCMFE under various scale factor

In this section, MFE and RCMFE of 90 groups of denoised HIFU echo signals are used for comparison and analysis, including 45 groups of denatured status and 45 groups of normal status. Where the embedding dimension $m = 3$, similar tolerance $r = 0.1$ standard deviation of the HIFU echo signal and delay time is 1. Figure 5 is the MFE and RCMFE of normal and denatured tissues under various scale factors. It can be seen that MFE or RCMFE parameters of normal and denatured tissues are distinguishable to some extent under various scale factors. In Fig. 5(b), there are relatively few overlapping points of RCMFE for the two statuses, which proves that RCMFE has a stronger aggregation capacity and nonlinearity than MFE, and it is relatively compact. However, this is not sufficient to fully determine that RCMFE is better than MFE in distinguishing tissues status, so the intra-class distance and the inter-class distance are introduced to demonstrate the superiority of RCMFE.

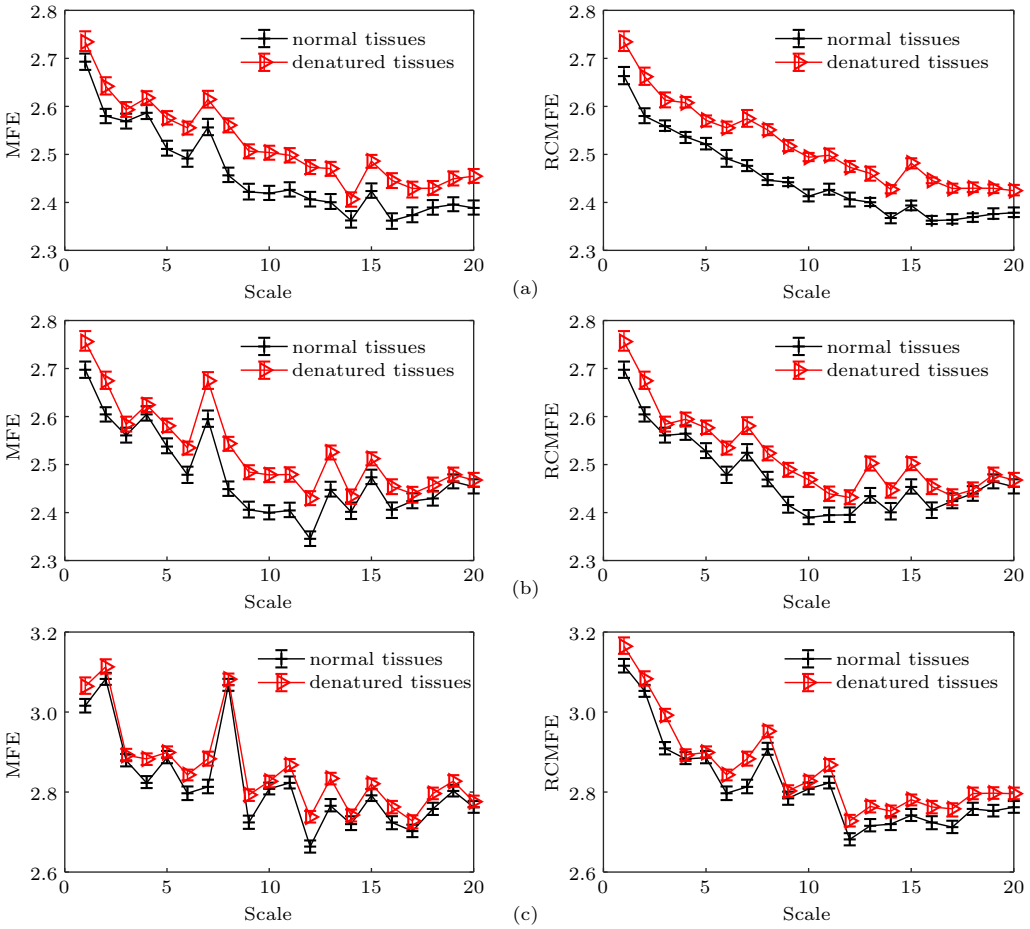


Fig. 4. MFE and RCMFE with different embedding dimensions. (a) $m = 3$; (b) $m = 4$; (c) $m = 5$.

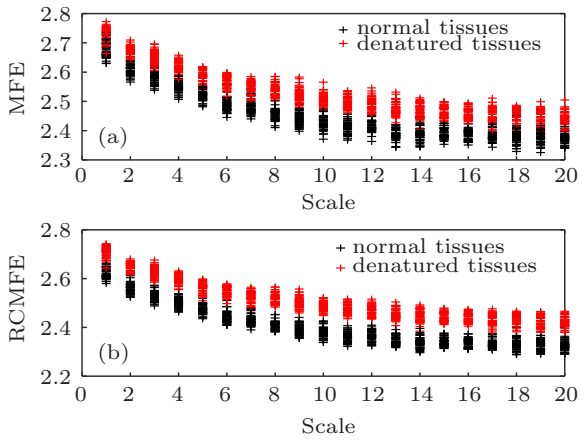


Fig. 5. MFE and RCMFE of denoised HIFU echo signals from normal and denatured tissues under various scale factors. (a) MFE; (b) RCMFE.

3.6. The intra-class distance and the inter-class distance of MFE and RCMFE

Figures 6 and 7 show the intra-class distance and inter-class distance of MFE and RCMFE under scale factor 1-20. The intra-class distance and the inter-class distance can reflect compactness and separability. If the intra-class distance is smaller and inter-class distance is larger, it proves that compactness and separability are better. It can be seen from Fig. 6 that the intra-class distance of RCMFE is significantly smaller than that of MFE, and the intra-class distance of RCMFE is the smallest under a scale factor of 16. Figure 7 shows a comparison of inter-class distance. It can be seen that the inter-class distance of RCMFE is higher than that of MFE, and the value under a scale factor of 16 is the largest. Therefore, when the scale factor is 16, RCMFE's intra-class distance is the smallest, and the inter-class distance is the largest, which can distinguish the denatured tissues from normal tissues.

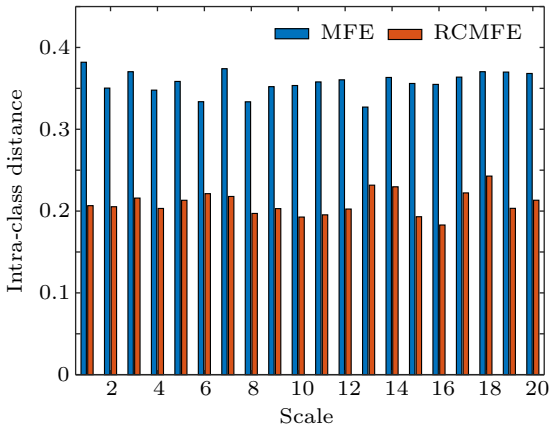


Fig. 6. Intra-class distance between MFE and RCMFE under various scale factors.

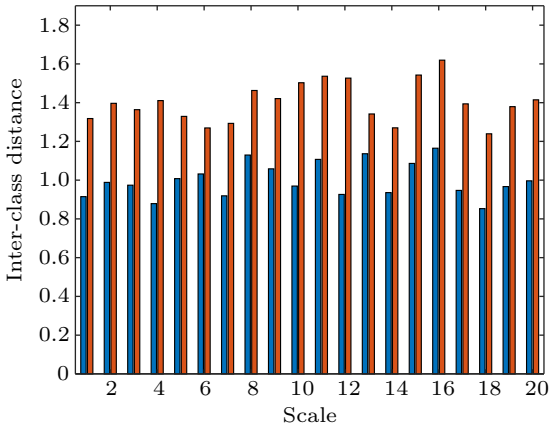


Fig. 7. Inter-class distance between MFE and RCMFE under various scale factors.

4. Conclusion

A novel method based on CS and RCMFE is proposed to identify the denatured and normal porcine tissues during HIFU treatment in this paper. CS with an improved observation matrix is used to denoise the HIFU echo signal, which can obtain a better denoising effect comparing to wavelet and EMD methods. Considering the weakness of MFE, refined composite is introduced into MFE, and RCMFE is proposed as a characteristic parameter. The influences of embedding dimensions and scale factors on MFE and RCMFE are analyzed. Through the calculation of them for the simulated signals and the denoised HIFU echo signals, the results show that RCMFE overcomes the disadvantage of large fluctuation, and RCMFE has smaller intra-class distance and larger inter-class distance than MFE, which has better compactness and separability in identifying tissues status. In addition, when the embedding dimension is selected as 3, and the scale factor is selected as 16, the optimal identification effect can be obtained during HIFU treatment. The results of this study revealed the differences in RCMFE between normal and denatured porcine tissues during HIFU treatment, which helps doctors to evaluate the treatment effect more accurately.

References

[1] Maloney E and Hwang J H 2015 *Int. J. Hyperthermia* **31** 302
[2] Cranston D 2015 *Ultrason. Sonochem.* **27** 654
[3] You Y F, Wang Z G, Ran H T, Zheng Y Y, Wang D, Xu J S, Wang Z B, Chen Y and Li P 2016 *Nanoscale* **8** 4324
[4] Bailey M R, Khokhlova V A, Sapozhnikov O A, Kargl S G and Crum L A 2003 *Acoust Phys.* **49** 369
[5] Kakiuchi T, Nakayama A, Nojiri J and Matsuo M 2019 *Intern. Med.* **58** 1965
[6] Ahmed H U, Bosaily A E S, Brown L C, Gabe R, Kaplan R, Parmar M K, Collaco-Moraes Y, Ward K, Hindley R G, Freeman A, Kirkham A P, Oldroyd R, Parker C and Emberton M 2017 *Lancet* **389** 815
[7] Yang C L, Zhu H, Wu S C, Bai Y P and Gao H J 2010 *J. Ultrasound Med.* **29** 1787
[8] Liu C C, Dong R, Li B Y, Li Y, Xu F, Ta D and Wang W Q 2019 *Chin. Phys. B* **28** 024302
[9] Paris M T, Bell K E, Avrutin E and Mourtzakis M 2020 *Clin. Physiol. Funct. Imaging* **40** 277
[10] Seip R, Tavakkoli J, Carlson R F, Wunderlich A, Sanghvi N T, Dines K A and Gardner T A 2002 *IEEE Ultrasonics Symposium*, October 8–11, 2002, Munich, Germany, p. 1427
[11] Donoho D L 2006 *IEEE Trans. Inf. Theory* **52** 1289
[12] Chen Y, Liu Z Q and Liu H L 2018 *IEEE Access* **6** 28318
[13] Ramdas V, Gorthi S S R K and Mishra D 2016 *Int. J. Speech Technol.* **19** 509
[14] Zhang P F, Deng M, Jing J N and Chen K 2020 *J. Appl. Geophys* **177** 104011
[15] Arildsen T and Larsen T 2014 *Signal Process.* **98** 275
[16] Mobasheri S, Behnam H, Rangraz P and Tavakkoli J 2016 *J. Med. Signals Sens.* **6** 91
[17] Richman J S and Moorman J R 2000 *Am. J. Physiol.-Heart Circul. Physiol.* **278** H2039
[18] Chen W T, Zhuang J, Yu W X and Wang Z Z 2009 *Med. Eng. Phys.* **31** 61
[19] Chen W T, Wang Z Z, Xie H B and Yu W X 2007 *IEEE Trans. Neural Syst. Rehabil. Eng.* **15** 266
[20] Liu C Y, Li K, Zhao L N, Liu F, Zheng D C, Liu C C and Liu S T 2013 *Comput. Biol. Med.* **43** 100
[21] Costa M, Goldberger A L and Peng C K 2005 *Phys. Rev. E* **71** 021906
[22] Costa M D, Goldberger A L 2015 *Entropy* **17** 1197
[23] Zheng J D, Cheng J S, Yang Y and Luo S R 2014 *Mech. Mach. Theory.* **78** 187
[24] Fadlallah B, Chen B, Keil A and Príncipe J 2013 *Phys. Rev. E* **87** 022911
[25] Wu S D, Wu C W, Lin S G, Wang C C and Lee K Y 2013 *Entropy* **15** 1069
[26] Wu S D, Wu C W, Lin S G, Lee K Y and Peng C K 2014 *Phys. Lett. A* **378** 1369
[27] Zheng J D, Pan H Y and Cheng J S 2017 *Mech. Syst. Signal Proc.* **85** 746
[28] Aldroubi A, Chen X M and Powell A M 2012 *Appl. Comput. Harmon. Anal.* **33** 282
[29] Do T T, Gan L, Nguyen N and Tran T D 2012 *IEEE Trans. Signal Process.* **60** 139
[30] Needell D and Vershynin R 2009 *Found. Comput. Math.* **9** 317
[31] Tropp J A and Gilbert A C 2007 *IEEE Trans. Inf. Theory* **53** 4655
[32] Kira K and Rendell L A 1992 *Tenth National Conference on Artificial Intelligence*, July 12, 1992, Atlanta, United States, p. 129
[33] Liu B, Qian S Y and Hu W P 2019 *Entropy* **21** 666
[34] Wang S S and Chen Y 2019 *Multidimens. Syst. Signal Process.* **30** 1517